RSC Advances

PAPER

View Article Online
View Journal | View Issue

Cite this: *RSC Adv.*, 2020, **10**, 42613

Low temperature selective catalytic reduction of nitric oxide with an activated carbon-supported zero-valent iron catalyst

Wan Cao and Weijun Zhang*

Selective catalytic reduction (SCR) of nitrogen oxides with an activated carbon-supported zero-valent iron catalyst is a method for removing NO under low temperature, which can remove CO and NO simultaneously. In the present study, the thermodynamics of low temperature denitrification was analyzed. By means of X-ray diffraction and Brunner–Emmet–Teller (BET) measurements, the phase and structure of the catalyst were thoroughly investigated. To determine the activity of the catalyst, a series of catalytic performance tests were carried out. The results indicated that the catalyst can act on the chemical reactions during the low-temperature denitrification process. An increase in the iron loading covered the micropores, resulting in a smaller specific surface area, which had little influence on the total pore volume. Moreover, activated carbon provided a carrier structure for iron and reduced NO simultaneously. The reduction of NO with activated carbon to N_2 was the main reaction. By the oxidation of iron and the reduction of activated carbon, the activity of the catalyst decreased.

Received 17th September 2020
Accepted 6th November 2020

DOI: 10.1039/d0ra07939a

rsc.li/rsc-advances

1. Introduction

Coal burning industries release large amounts of nitrogen oxides, which is one of the environmental problems solved seriously. Nitrogen oxides cause numerous hazards, such as acid rain, smog and human diseases. NO is the main component of nitrogen oxides in flue gas, and at present, SCR is considered as a promising technology for removing NO. SCR is widely used in the thermal power industry to remove NO, but the sintering process and smoke extraction in other industries also produce copious amounts of NO. The smoke extraction temperature in industries is in the temperature range of 20–180 °C, and the best catalytic activity of the catalyst in the SCR is in the temperature range of 380–450 °C. The activity of the catalyst is greatly reduced when the active temperature window of the catalyst does not match with the low temperature. Heating the flue gas to remove NO_x will result in a waste of energy and increase the operating costs of enterprises. In order to solve the problem, the emission reduction of nitrogen oxides from low-temperature sintering flue gas has been developed.

The core of low temperature denitrification is to select reductants and catalysts with high activity at low temperatures. Current studies have shown that supported catalysts have excellent activity, such as carbon-supported metal oxides,[1,2] cordierite-supported MnO_x–CuO_x,[3] Al_2O_3-supported Ag and MgO,[4] TiO_2-supported Mn and Fe,[5] ZSM-5-supported mixture of Fe, Ce and Mn,[6] CNT-supported mixture of Mn and FeO_x.[7] A supported catalyst consists of two parts: a carrier and an active component. The carrier can provide a large specific surface area and pore diameter structure, which can improve the stability of the catalyst. The active component plays an important role of denitrification. Metals, metal oxides and composite compounds can be used as the active components.[5,8,9] SCR takes the advantage of the interaction between the reducing agent and the catalyst. Among them, most of the reductants are gases and only a few are liquids, almost no solids, such as hydrocarbons,[4] CO,[10,11] H_2O_2,[12] NH_3 and urea.[1,13–15] Zhao and Yuan *et al.* used an extra system to vaporize H_2O_2.[12] H_2O_2 in the gaseous state was more efficient than in the liquid state, but vaporization devices increased the cost of removing NO. As NH_3-SCR, most denitrification temperatures were higher than 150 °C.[16–19] Besides, using NH_3 as the reductant can result in an NH_3 slip. For example, during the actual process of coal removing NO_x, the NH_3 slip is in the range of 2–5 ppm.[16] Therefore, the screening for stable reducing agents and synthesizing economical and efficient catalysts for removing NO_x at low temperatures have attracted attention.

Iron-based materials are inexpensive, readily available and non-toxic, and they have been studied at low temperatures for removing NO_x. Yang and Wang *et al.* studied a low-temperature selective catalytic reduction of NO with NH_3 over Fe and Mn.[19] Liu and Wang *et al.* used a metal oxide-containing iron ($Fe_2(MoO_4)_3$) to remove NO and SO_2.[20] Molecular sieves, ceramics, zeolites and activated carbon are often used as carriers; however, activated carbon with a large specific surface area and a complex pore structure is the most commonly used. In order to have a higher specific surface area and a more suitable pore size structure, activated carbon deforms into different shapes, such as

School of Metallurgy, Industrial Furnace Research Institute, Northeastern University, Shenyang, 110819, P. R. China. E-mail: zhangwj@smm.neu.edu.cn

activated carbon fiber, activated carbon honeycomb and activated carbon ball.[21] Mochida and Kawano *et al.* treated a low amount of NO in air with an asphalt-based activated carbon fiber.[22] Ma and Yamamoto *et al.* coated the catalyst in the honeycomb to treat NO at low temperatures.[23] However, the preparation of the composite catalyst is complex, and the cost is also high. Hence, a catalyst with a low operating cost and high efficiency at a low temperature has attracted the attention of researchers.

In this study, to solve the problem of the nitrogen oxide removal in a low-temperature sintering flue gas, zero-valent iron was directly supported on activated carbon as a new type denitrification catalyst. The low temperature denitrification performance of the catalyst was studied by a series of denitrification activity tests. Moreover, to speculate the NO conversion mechanism, the thermodynamics of the low temperature denitrification was also analysed. By means of X-ray diffraction and BET techniques, the phase and structure of the catalyst were thoroughly investigated.

2. Thermodynamics

Scholars focus on the kinetic analysis of SCR, while the thermodynamic analysis has not been discussed yet. Moreover, the experimental conditions and the catalyst in this paper are different from those in the previous studies. For any catalyst, it can only catalyze spontaneous reactions. Under isothermal and isobaric conditions, the Gibbs free-energy (ΔG) change is used to determine the direction of the reaction. The limit is measured by the chemical equilibrium constant (K_c).[24]

The Gibbs free-energy (ΔG) and the chemical equilibrium constant (K_c) is expressed as:

$$\Delta G = \Delta H - T\Delta S$$

$$K_c = \exp(-\Delta G/RT)$$

where ΔH (J mol^{-1}) is the enthalpy change of the reaction; T is the reaction temperature; ΔS (J (mol K)$^{-1}$) is the entropy change of the reaction; R is the gas constant (8.314 J (mol K)$^{-1}$).

According to the above formulae and using the reaction equation module of the HSC Chemistry 6.0 thermodynamic calculation software, the thermodynamic calculations of chemical reactions involved in the low-temperature denitrification process were carried out. The reaction temperature was in the range of 25–100 °C, one interval was 5 °C, and the reaction pressure was 101.325 kPa.

Based on the catalytic mechanism of Eley–Rideal and Mars–van Krevelen,[25,26] the flowing reactions might take place on the surface and in the inner hole of the catalyst:

$$C + NO \rightarrow CO + N_2 \quad (1)$$

$$C + NO \rightarrow CO_2 + N_2 \quad (2)$$

In the presence of CO, it is reductive and can reduce nitrogen oxides:

$$CO + NO \rightarrow N_2 + CO_2 \quad (3)$$

Besides, in the sintering flue gas, the amount of oxygen is high, and the following reaction will occur in the presence of sufficient amount of oxygen:

$$NO + O_2 \rightarrow NO_2 \quad (4)$$

The amount of carbon substrate in the catalyst is sufficient to reduce NO in the flue gas, and NO_2 is produced by side reactions:

$$NO_2 + C \rightarrow N_2 + CO \quad (5)$$

$$NO_2 + C \rightarrow N_2 + CO_2 \quad (6)$$

$$NO + NO_2 + C \rightarrow N_2 + CO \quad (7)$$

$$NO + NO_2 + C \rightarrow N_2 + CO_2 \quad (8)$$

As shown in Fig. 1, the Gibbs free-energies in the chemical reaction processes from (1)–(8) were negative, indicating that the above chemical processes were spontaneous. Among them, ΔG of reaction (2) was smaller than that of reaction (1), and lg K_c was larger, indicating that the reaction between NO and carbon was easier to proceed as reaction (2). Similarly, the comparison between reaction (6) and reaction (5) and the comparison between reaction (8) and reaction (7) indicated that the reactions of CO_2 products with the same reactants is more likely to occur than those with CO. In Fig. 1, the equilibrium constant of reaction (4) is the smallest and its Gibbs free-energy change ΔG is the largest, indicating that reaction (4) is the most difficult to occur of all the possible chemical reactions. Alternatively, NO oxidized to NO_2 by O_2 is the slowest step in the whole process of low-temperature denitrification. Although the oxygen content of the sintered flue gas is higher than other industrial flue gases, it was difficult to promote the forward progress of reaction (4). In addition, it can be seen from Fig. 1 that reaction (6) is most likely to occur at a low temperature. However, since NO in the flue gas accounted for more than 90% of all nitrogen oxides, reaction (8) was more likely to occur in the actual low-temperature removing NO_x process. According to reaction (3), CO promoted denitrification at a low temperature. The reduction of NO to N_2 by activated carbon was the main reaction in the low-temperature removing NO_x (reaction (3)). Reaction (2) was an auxiliary chemical reaction process of denitrification, it could promote the conversion of NO to N_2 and simultaneously remove CO from the flue gas. In conclusion, as a catalytic denitrification material, the activated carbon-supported zero-valent iron catalyst could act on the above spontaneous chemical reactions. The process of low-temperature denitrification could be promoted by using CO in the sintering flue gas, and the harmful CO gas could be disposed simultaneously.

3. Experimental

3.1. Materials

The main raw materials were carbon powder and iron ore powder with particle size of 120–160 mesh. Carbon powder was blue carbon power with dry-base-fixed carbon more than 75%.

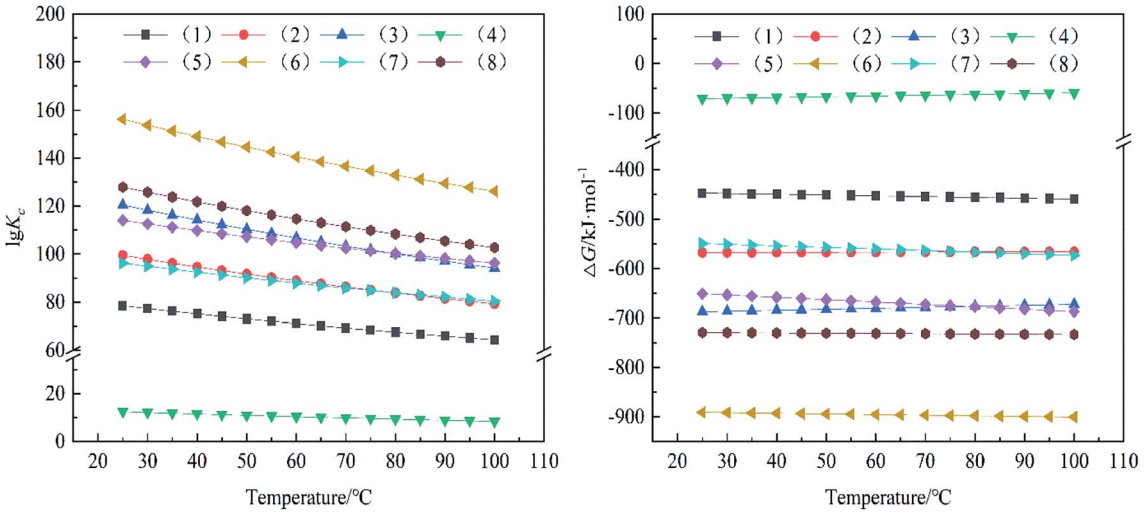

Fig. 1 Relation of the chemical equilibrium constant and the Gibbs free-energy change of temperature and experimental reaction.

The above raw materials were purchased from Liaoning Boliante Metallurgical Technology Co., LTD.

According to the ratio, carbon powder, iron ore powder and binder (1–2% of binder, particle size is 200 mesh) were put into a star wheel mixer for mixing and rolling. Raw pellets with diameters in the range of 12–18 nm formed by the disk-type pelletizing mechanism, and the unqualified pellets were screened out. The qualified pellets were dried at 110 °C (the water content was controlled below 5%). The dried pellets were put into a can, a 20% small particle residual carbon was used as buffer during canning. The canister was sealed with residual carbon. The pellets were calcined in a shuttle kiln at 1050 °C for 8–10 h. After the calcining process, the pellets were cooled naturally in the kiln and discharged when the temperature was below 100 °C.

3.2. Methods

3.2.1. BET analysis. BET surface areas of carbon materials were measured by N_2 adsorption isotherm at 77 K using an ASAP 2020 Plus. The total pore volume was obtained by the BJH method, and the pore size was obtained by analysing the isothermal adsorption curve.

3.2.2. X-ray diffraction. The composition of grains and materials formed on the surface of the catalyst was observed *via* X-ray diffraction (XRD) using a Panaco, (Netherlands) with the Cu Kα radiation ($k = 1.54056$ Å) in the 2θ range of 10°–90°, with a step length 0.02.

3.3. Catalytic performance tests

The experiments for SCR of NO were carried out in a fixed-quartz reactor (1200 mm high with a diameter of 180 mm) in the temperature range of 25–60 °C. The resistance furnace could effectively control the temperature constant. Steel plates with holes were placed at the bottom of the reactor to prevent pellets from falling off and clogging the line. A measured amount of catalyst (i.d. 12–18 nm) was placed into the reactor. The catalyst

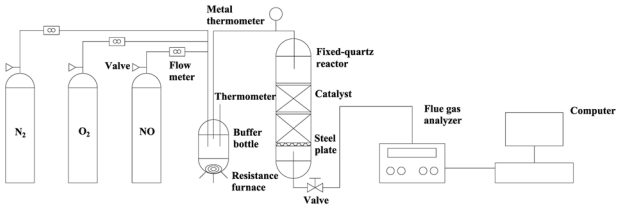

Fig. 2 Installation drawing of the performance tests.

was purged *in situ* by passing N_2 for 30 min at the reaction temperature. The tests of the activity were performed with a mixture of NO (230 ppm) and O_2 (20 vol%) balanced by N_2, and the total intake flow was 1800 L min^{-1}. The performance tests flow chart is shown in Fig. 2. A flue gas analyser (Germany MRU infrared flue gas analyser, MGA6) was used for analysing the concentrations of the import and export NO_x. The NO_x conversions were calculated according to the following formula:

$$NO_x \text{ conversion} = \frac{C_{NO_{inlet}} - C_{NO_{outlet}}}{C_{NO_{inlet}}} \times 100\%$$

Among which, NO_{inlet} is the concentration of nitric oxide (NO) at the inlet of the reactor, NO_{outlet} is the concentration of nitrogen oxides (NO) at the outlet of the reactor.

4. Results and discussion

4.1. Pore size distribution and BET tests

The specific surface areas and the pore structure parameters were obtained *via* the BET and BJH models, respectively. As shown in Table 1, the specific surface area of C_1-ZFe_4 is the largest. As the proportion of iron decreased, the specific surface area of the catalyst increased. The average pore diameter of C_1-ZFe_1 is the smallest, and the average pore diameter of the catalyst increased with an increase in the iron proportion. The

Table 1 Specific surface areas and pore structure parameters at different raw material ratios[a]

Sample	S_{BET} ($m^2\ g^{-1}$)	V_{total} ($cm^3\ g^{-1}$)	$V_{micropore}$ ($cm^3\ g^{-1}$)	D_{pore} (nm)
C_1-ZFe_4	19	0.03	0.000	4.34
C_1-$ZFe_{2.3}$	55	0.06	0.008	4.22
C_1-$ZF_{1.5}$	78	0.07	0.016	4.17
C_1-ZFe_1	86	0.06	0.022	3.26

[a] C_a-ZFe_b, a and b represent the ratio of the mass fraction of carbon and iron ore powder during pellets preparation (20 : 80; 30 : 70; 40 : 60; 50 : 50), and the carbon ratio is turned into a convenient comparison.

above results indicated that with an increase in the iron proportion, the zero-valent iron was mainly filled in the micropores of the activated carbon, leading to a decrease in the micropores and specific surface area of the catalyst. It was consistent with the micropore volume data in Table 1. For the total pore volume, the proportion of iron had a little influence on the total pore volume except C_1-ZFe_4. It also showed that the proportion of iron mainly affected the micropores.

Fig. 3 illustrates the pore diameter distributions and nitrogen adsorption isotherms of C_1-ZFe_4, C_1-$ZFe_{2.3}$, C_1-$ZF_{1.5}$ and C_1-ZFe_1. For C_1-ZFe_4, when the relative pressure is less than 0.03, no nitrogen adsorption occurred, while the other three catalysts quickly adsorbed N_2 in this pressure zone. The results showed that the process of filling the micropores on the catalyst increased with a decrease in the iron proportion. At medium relative pressure, there was a distinct plateau of C_1-ZFe_1, indicating that almost no mesopores existed in C_1-ZFe_1. At high relative pressure, capillary condensation occurred in all catalysts except C_1-$ZF_{1.5}$, which should be related to its characteristic of the largest total pore volume. For the pore diameter distributions of the catalysts, no pores were less than 2 nm in C_1-ZFe_4, all of which were mesoporous. The N_2 adsorption of C_1-$ZFe_{2.3}$ and C_1-$ZF_{1.5}$ came from the interaction of micropores and mesopores, in which the C_1-$ZF_{1.5}$ pore size was mainly concentrated in the 2–6 nm range. C_1-ZFe_1 had no mesoporous pores.

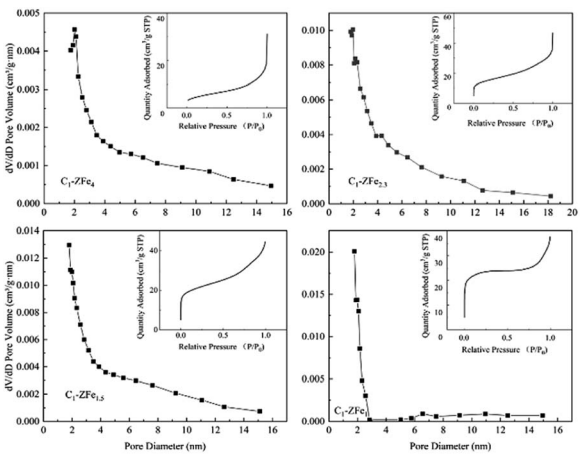

Fig. 3 Pore diameter distributions and nitrogen adsorption isotherms of C_1-ZFe_4, C_1-$ZFe_{2.3}$, C_1-$ZF_{1.5}$ and C_1-ZFe_1.

4.2. X-ray diffraction studies

The X-ray powder diffraction of C_1-ZFe_4 before and after absorbing NO were recorded, as shown in Fig. 4. From Fig. 4, the phase of C_1-ZFe_4 changed obviously before and after absorbing NO. The main crystalline phases were zero-valent iron (PDF no. 06-0696) and ferroferric oxide (PDF no. 28-0491, zero-valent iron in 2θ 44.7, 65.4 and 82.3, ferroferric oxide represents a mixture of iron, ferrous and ferric). In Fig. 4, the peak strength of the phase had no change before and after the removal of NO, indicating that zero-valent iron did not participate in the chemical reaction process at this time. In the whole process of removing NO at a low temperature, iron was used as the catalyst to facilitate the reduction of NO by activated carbon. The use of transition metals as the catalysts has been documented in some literature.[10,27,28] In addition, activated carbon as a structural carrier provided a suitable porous loading structure for iron. The denitrification process was mainly determined by the reducibility of activated carbon and the catalysis of elemental iron.

4.3. Catalytic cycle test

To determine the life of the catalyst, cycle experiments were carried out. We conducted the cycle experiments for C_1-ZFe_4 with 230 ppm NO and 20 vol% O_2 at 30 °C. The results of the cycle experiments are shown in Fig. 5. It can be seen from Fig. 5 that the activity of C_1-ZFe_4 decreased gradually with the increase in the denitrification time in each experiment. After 180 min of

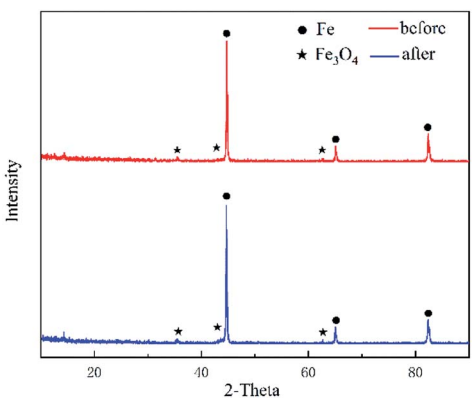

Fig. 4 XRD patterns of C_1-ZFe_4 before and after absorbing NO.

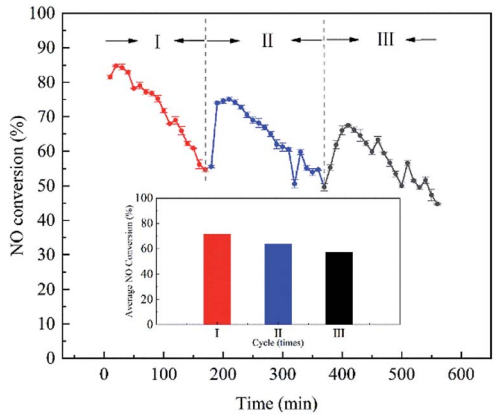

Fig. 5 Performance of C_1-ZFe_4 for cycle tests.

each trial, the activity of the catalyst decreased about 35%. In addition, the average NO conversion of the catalyst decreased with the increase in cycle times, indicating that C_1-ZFe_4 was a consumable catalyst. It can be seen from Table 1 that the mesoporous distribution of C_1-ZFe_4 was relatively large, and the deactivation of C_1-ZFe_4 had nothing to do with the blockage of the sulphate. Combining the information of the thermodynamic process and Fig. 4, we considered that the deactivation of C_1-ZFe_4 occurred due to two reasons: one was the oxidation of iron, and the other was the reduction of activated carbon. The zero-valent iron lost its catalytic activity after oxidation. The reduction of nitric oxide in the activated carbon was the main reaction in the process of removing NO in the low temperature. The reduction influenced the efficiency inevitably. Because of the resistance to water vapor and SO_2, most catalysts deactivate.[20] For NH_3-SCR, ammonium sulphate was produced to clog the structure of the catalyst. The deactivation mode of the catalyst in this study was not determined by SO_2. We believe that the catalyst had a good SO_2 resistance. This part will be discussed in detail in other articles.

5. Conclusions

The activated carbon-supported zero-valent iron is a novel catalyst for the selective catalytic reduction of nitric oxide at a low temperature, which can resist the harm of CO, remove CO and NO simultaneously. The main conclusions obtained in the present research are as follows:

(1) as a catalytic denitrification material, the activated carbon-supported zero-valent iron catalyst could act on spontaneous chemical reactions. The reaction of NO oxidized to NO_2 was the slowest step in the whole process. NO reduction by activated carbon was the main reaction of the denitrification process. CO could promote the conversion of NO to N_2.

(2) With the increase in iron proportion, the zero-valent iron mainly affected the micropores of activated carbon, leading to the decrease in the micropores and the specific surface area of the catalyst. The proportion of iron had a little influence on the total pore volume.

(3) In the process of the low temperature denitrification, iron was used as the catalyst to catalyze the reduction of NO by activated carbon. Activated carbon provided a porous loading structure for iron.

(4) The activity of the catalyst was reduced when the catalyst was used numerous times. It was because the catalysis of iron and the reduction of activated carbon were decreased.

Conflicts of interest

There are no conflicts to declare.

Acknowledgements

This work was supported by the National Key Research and Development Program of China [project number 2017YFA0700300].

Notes and references

1 K. Liu, Q. Yu, B. Wang, *et al.*, Low temperature selective catalytic reduction of nitric oxide with urea over activated carbon supported metal oxide catalysts, *Environ. Technol.*, 2020, **41**, 808–821.

2 Y. Wang, C. Ge, L. Zhan, *et al.*, MnO_x–CeO_2/Activated Carbon Honeycomb Catalyst for Selective Catalytic Reduction of NO with NH_3 at Low Temperatures, *Ind. Eng. Chem. Res.*, 2012, **51**, 11667–11673.

3 Z. Lei, S. Hao, L. Zhang, *et al.*, MnO_x-CuO_x cordierite catalyst for selective catalytic oxidation of the NO at low temperature, *Environ. Sci. Pollut. Res.*, 2020, **27**, 23695–23706.

4 P. M. More, N. Jagtap, A. B. Kulal, *et al.*, Magnesia doped Ag/Al_2O_3-Sulfur tolerant catalyst for low temperature HC-SCR of NO_x, *Appl. Catal., B*, 2014, **144**, 408–415.

5 S. S. R. Putluru, L. Schill, A. D. Jensen, *et al.*, Mn/TiO_2 and Mn–Fe/TiO_2 catalysts synthesized by deposition precipitation—promising for selective catalytic reduction of NO with NH_3 at low temperatures, *Appl. Catal., B*, 2015, **165**, 628–635.

6 G. Zhou, B. Zhong, W. Wang, *et al.*, In situ DRIFTS study of NO reduction by NH_3 over Fe–Ce–Mn/ZSM-5 catalysts, *Catal. Today*, 2011, **175**, 157–163.

7 Y. Zhang, Y. Zheng, W. Xie, *et al.*, Preparation of Mn–FeO_x/CNT_s catalysts by redox co-precipitation and application in low-temperature NO reduction with NH_3, *Catal. Commun.*, 2015, **62**, 57–61.

8 S. Cai, H. Hu, H. Li, *et al.*, Design of multi-shell Fe_2O_3@$MnO_{(x)}$@CNT_s for the selective catalytic reduction of NO with NH_3: improvement of catalytic activity and SO_2 tolerance, *Nanoscale*, 2016, **8**, 3588–3598.

9 J. Alcañiz-Monge, A. Bueno-López, M. Á. Lillo-Rodenas, *et al.*, NO adsorption on activated carbon fibers from iron-containing pitch, *Microporous Mesoporous Mater.*, 2008, **108**, 294–302.

10 K. Liu, Q. Yu, T. Wu, *et al.*, Manganese-based catalyst for NO removal at low temperatures: thermodynamics analysis and

experimental, validation, *Pet. Sci. Technol.*, 2018, **36**, 1663–1671.

11 Y. H. Qin, L. Huang, J. X. Zheng, *et al.*, Low-temperature selective catalytic reduction of NO with CO over A-Cu-BTC and AO_x/CuO_y/C catalyst, *Inorg. Chem. Commun.*, 2016, **72**, 78–82.

12 Y. Zhao, B. Yuan, R. Hao, *et al.*, Low-Temperature Conversion of NO in Flue Gas by Vaporized H_2O_2 and Nanoscale Zerovalent Iron, *Energy Fuels*, 2017, **31**, 7282–7289.

13 J. M. García-Cortés, J. Pérez-Ramírez, M. J. Illán-Gómez, *et al.*, Comparative study of Pt-based catalysts on different supports in the low-temperature de-NO_x-SCR with propene, *Appl. Catal., B*, 2001, **30**, 399–408.

14 J. Kašpar, P. Fornasiero and N. Hickey, Automotive catalytic converters: current status and some perspectives, *Catal. Today*, 2003, **77**, 419–449.

15 M. Koebel, M. Elsener and M. Kleemann, Urea-SCR: a promising technique to reduce NO_x emissions from automotive diesel engines, *Catal. Today*, 2000, **59**, 335–345.

16 Z. Liang, X. Ma, H. Lin, *et al.*, The energy consumption and environmental impacts of SCR technology in China, *Appl. Energy*, 2011, **88**, 1120–1129.

17 M. Barreau, M. L. Tarot, D. Duprez, *et al.*, Remarkable enhancement of the selective catalytic reduction of NO at low temperature by collaborative effect of ethanol and NH_3 over silver supported catalyst, *Appl. Catal., B*, 2018, **220**, 19–30.

18 W. Tian, H. Yang, X. Fan, *et al.*, Catalytic reduction of NO_x with NH_3 over different-shaped MnO_2 at low temperature, *J. Hazard. Mater.*, 2011, **188**, 105–109.

19 S. Yang, C. Wang, J. Li, *et al.*, Low temperature selective catalytic reduction of NO with NH_3 over Mn–Fe spinel: performance, mechanism and kinetic study, *Appl. Catal., B*, 2011, **110**, 71–80.

20 X. Liu, C. A. Wang, T. Zhu, *et al.*, Simultaneous removal of NO and SO_2 from coal-fired flue gas based on the catalytic decomposition of H_2O_2 over $Fe_2(MoO_4)_3$, *Chem. Eng. J.*, 2019, **371**, 486–499.

21 M. Busch, A. Kompch, S. Suleiman, *et al.*, NO_x conversion properties of a novel material: iron nanoparticles stabilized in carbon, *Appl. Catal., B*, 2015, **166–167**, 211–216.

22 I. Mochida, S. Kawano, M. Hironaka, *et al.*, Reduction of NO of Very Low Concentration in Air with NH_3 at Room Temperature over Calcined Active Carbon Fibers, *Energy Fuels*, 1995, **9**, 659–664.

23 H. Ma, Y. Yamamoto, J. Yu, *et al.*, SCR catalyst coated on low-cost monolith support for flue gas denitration of industrial furnaces, *Chem. Eng. J.*, 2013, **230**, 513–521.

24 H. Yi, H. Deng, X. Tang, *et al.*, Adsorption equilibrium and kinetics for SO_2, NO, CO_2 on zeolites FAU and LTA, *J. Hazard. Mater.*, 2012, **203–204**, 111–117.

25 C. Songying, *Engineering Foundation of Catalytic Reaction*, Chemical Industry Press, Beijing, 2011.

26 B. Tongchun, *Physical and Chemical*, Nanjing University Press, Nanjing, 2015.

27 M. Ye, C. Cheng, Y. Li, *et al.*, Enhancement of the denitrification efficiency over low-rank activated coke by doping with transition metal oxides, *Can. J. Chem. Eng.*, 2020, **98**, 1390–1397.

28 H. Liu, J. Yang, X. Qiao, *et al.*, Microwave Plasma-Assisted Catalytic Reduction of NO by Active Coke over Transition-Metal Oxides, *Energy Fuels*, 2020, **34**, 4384–4392.

